

Dust depletion and abundance pattern in damped Ly α systems: a sample of Mn and Ti abundances at $z < 2.2^*$

Cédric Ledoux¹, Jacqueline Bergeron¹, and Patrick Petitjean^{2,3}

¹ European Southern Observatory, Karl-Schwarzschild Straße 2, D-85748 Garching bei München, Germany

e-mail: cledoux@eso.org, jbergero@eso.org

² Institut d'Astrophysique de Paris, 98bis Boulevard Arago, F-75014 Paris, France

e-mail: petitjean@iap.fr

³ DAEC, Observatoire de Paris-Meudon, F-92195 Meudon Principal Cedex, France

Received 3 August 2001 / Accepted 4 February 2002

Abstract. We analyse a sample of 24 damped Lyman- α (DLA)/moderate DLA systems at intermediate redshifts, $0.3 < z_{\text{abs}} < 2.2$, all with measurement of the weak Mn II absorption lines, to investigate which elemental ratios could possibly be used as tracers of either dust depletion or nucleosynthesis effects. We applied a component-by-component analysis to the five systems of the sample with new observations and, using this procedure, re-analyzed data gathered from the literature whenever possible. We show that the standard method which uses column densities integrated over the whole absorption profiles could substantially underestimate the abundance of rare elements relative to Fe. We find a correlation between the observed [Si/Fe] and [Zn/Fe] ratios, present in our sample at the 2.9σ significance level. This correlation is fully consistent with a dust depletion sequence only for a Galactic warm disk cloud or halo cloud depletion pattern. The correlation between [Mn/Fe] and [Zn/Fe], detected at the 3.2σ significance level, cannot be accounted for by any dust depletion sequence: it implies either variations of the intrinsic Mn abundance relative to Fe from -0.3 to $+0.1$ dex and/or a relation between depletion level and metallicity. The correlation between [Mn/Fe] and metallicity (2.6σ significance level) strengthens the assumption of intrinsic variations of [Mn/Fe] although some marginal correlation between [Zn or Si/Fe] and [Zn/H] is present as well. Extension of the sample toward low metallicity is needed to confirm the correlation between depletion level and metallicity. The variations of [Ti/Fe] vs. [Zn/Fe] cannot be fitted by a single dust depletion sequence either. We then adopt a warm disk cloud or halo cloud depletion pattern and compare the resulting dust-corrected abundance ratios to those observed in Galactic and SMC stars. At high metallicity, $[\text{Fe}/\text{H}]_{\text{dc}} \gtrsim -0.5$, the intrinsic abundance pattern of Si, Ti, Cr and Mn in DLA absorbers closely follows the trends observed in Galactic stars and these absorbers should thus have a chemical evolution similar to that of our Galaxy. At lower metallicity, some absorbers do follow the trends present in Galactic stars but a substantial fraction of them have elemental ratios (in particular $[\text{Si}/\text{Fe}]_{\text{dc}}$ and $[\text{Mn}/\text{Fe}]_{\text{dc}}$) closer to the solar values than Galactic stars. This could be explained by a larger contribution of type Ia supernovae to the chemical enrichment of these DLA absorbers than in Galactic stars of similar metallicity. This metal-poor DLA absorber population could trace H I-rich dwarf galaxies.

Key words. Cosmology: observations – Galaxies: halos – Galaxies: ISM – Quasars: absorption lines

1. Introduction

The association of damped Lyman- α (DLA) systems with galaxies, as first suggested by Wolfe et al. (1986), has been demonstrated at low and intermediate redshifts by the

identification of a small sample of DLA systems at $z_{\text{abs}} \lesssim 1$ (Le Brun et al. 1997). These absorbers have been extensively used to probe the chemical history and the properties of the gaseous halos of distant galaxies. Their metallicity was first derived from high-resolution spectroscopic observations of Zn II absorption lines as this element is not significantly depleted onto dust grains in the Galactic interstellar medium (ISM). The derived $N(\text{H I})$ -weighted mean metallicity of DLA systems at $z_{\text{abs}} \gtrsim 2.5$ is about $1/13Z_{\odot}$ with a large spread of two orders of magnitude (Pettini et al. 1997b). The value found at $z_{\text{abs}} < 1.5$ is only slightly larger, $\sim 1/10Z_{\odot}$ (Pettini et al. 1999). These

Send offprint requests to: C. Ledoux

* Based on observations carried out at the European Southern Observatory (ESO), La Silla, under prog. ID No. 56.B-0261 and 59.B-0797, and during Science Verification of the UVES instrument at the ESO Very Large Telescope, Paranal (Chile). Also based on Hubble Space Telescope data retrieved from the Space Telescope European Coordinating Facility archive.

low metallicities point toward young galaxies, although the exact nature of high-redshift DLA systems is still controversial (see Prochaska & Wolfe 1997a; Ledoux et al. 1998). The wide range in metal enrichment and lack of significant evolution could be due to the presence of various populations of galaxies of different morphological types among the DLA absorbers, thus different star-formation histories.

The underabundance of Cr relative to Zn has been first attributed to the selective depletion of Cr onto dust grains (Pettini et al. 1994) by analogy to the Milky Way. Indeed, the high elemental abundance ratios $[Zn/Cr]$ ($\equiv \log[N(Zn)/N(H)] - \log[N(Cr)/N(H)]$) and/or $[S/Cr]$ in DLA systems with detected H_2 molecules demonstrates the presence of dust in these DLA absorbers (Ledoux et al. 2002; Petitjean et al. 2002). However, this interpretation has been challenged by Lu et al. (1996) and Prochaska & Wolfe (1997b). These authors studied the abundances of a large number of elements and suggested that the observed relative abundances may reflect the nucleosynthesis pattern of type II supernovae enrichment. It seems that several groups now tend to agree that both effects are present and that the $[Cr/Zn]$ ratio is primarily an indicator of dust depletion (Pettini et al. 1997a; Kulkarni et al. 1997; Vladilo 1998; Prochaska & Wolfe 1999).

The main goal of this paper is to analyze a large sample of DLA systems at intermediate redshift to investigate these issues further. We search for a clear depletion pattern, in particular for elements less depleted than Fe in the Galactic ISM other than Zn, as Si. We then concentrate our analysis on Mn and Ti, elements which have not been extensively studied so far. Our sample of 24 DLA/moderate-DLA absorbers combines new high spectral resolution data on five systems at $z_{\text{abs}} < 1.2$ with previously published data on DLA/moderate-DLA systems at $0.3 < z_{\text{abs}} < 2.2$. In all cases, the wavelength range of the expected, associated Mn II transition lines has been observed.

We describe our observations in Sect. 2 and present our analysis of individual absorbers and our measurements in Sects. 3 and 4, emphasizing the importance of component-by-component analysis. In Sect. 5, we discuss the abundance pattern observed in DLA systems. As explained in Sect. 6, we then correct the observed abundance ratios for dust depletion effects to finally draw our conclusions in Sect. 7.

2. Observations and data reduction

2.1. HST FOS spectra

UV spectra were retrieved from the HST Faint Object Spectrograph (FOS) archive to determine the $H\text{I}$ column density from the Lyman- α line of the metal-rich absorbers toward Q 0058+019 (PHL 938), Q 0453-423 and Q (PKS) 2128-123. The observation log is summarized in Table 1. The spectra were reduced again using the best reference files available for on-the-fly re-calibration

as provided by the Hubble Space Telescope European Coordinating Facility data reduction pipeline.

In the cases of Q 0058+019 and Q 2128-123, it was necessary to correct for scattered light for bringing the cores of the Lyman- α lines to the zero flux level (correction $< 10\%$). The signal-to-noise ratio in the adjacent continuum is of the order of 5 and 10 for Q 0058+019 and Q 2128-123 respectively. For Q 0453-423, no flux is actually observed in the G190H spectrum as is also the case shortward of about 3020 Å in the G270H spectrum, thereby revealing the existence of an optically thick Lyman-limit system at $z_{\text{abs}} \approx 2.3$ along the line of sight.

2.2. VLT UVES data

High-resolution, high signal-to-noise ratio spectra were obtained with the UV and Visible Echelle Spectrograph (UVES) at the Kueyen VLT-UT2 8.2 m telescope on Cerro Paranal Observatory during UVES Science Verification (SV; February 6-17, 2000). Combining two standard dichroic settings: Dic#1 (grisms B346nm, R580nm) and Dic#2 (grisms B437nm, R860nm), to observe with both spectrograph arms, the full optical range was covered from ~ 3050 to 10000 Å with only a small gap between the two red CCDs (see Table 1). A slit width of $0''.9$ (resp. $0''.8$) in the Blue (resp. Red) was used in good seeing conditions and of $1''.0$ when the seeing was poor, yielding a spectral resolution $42500 < R < 50000$.

The calibrated data for Q 1122-168 was made available to the ESO community in May 2000. The data reduction was performed by the SV team using the UVES pipeline (Ballester et al. 2000), available as a context of the MIDAS software. The main characteristics of the pipeline is to perform a precise inter-order background subtraction, especially for master flat-fields, and to allow for an optimal extraction of the object signal rejecting cosmic rays and performing sky-subtraction at the same time. The pipeline results were checked step by step. We then converted the wavelengths of the reduced spectra to vacuum-heliocentric values and scaled, weighted and combined individual 1D exposures using the NOAO *onedspec* package of the IRAF software. The resulting unsmoothed spectra were re-binned to the same wavelength step ($0.0415 \text{ \AA pix}^{-1}$), yielding a signal-to-noise ratio per resolution element of 100 (resp. 37) at 5500 Å (resp. 4000 Å).

2.3. ESO CASPEC data

High-resolution spectroscopy data of three quasars, Q 0058+019, Q 0453-423 and Q 2128-123, were obtained with the CASPEC echelle spectrograph at the ESO 3.6 m telescope at La Silla Observatory on November 18-21, 1995 and September 23-26, 1997. The observational details are summarized in Table 1. A spectral range of 1200 Å was covered per setting. The instrumental resolution FWHM is 0.16 \AA (or 11 km s^{-1}) and the accuracy in the

wavelength calibration is of the order of one tenth of the resolution.

The data were reduced and analyzed using the *echelle* package of MIDAS. The object-flux weighted median of individual frames and cosmic-ray removal were performed simultaneously. The sky spectrum was difficult to extract in the blue due to the small spacing between orders. We thus carefully fitted the zero level to the bottom of the saturated lines in the extracted 1D spectra. The uncertainty in the flux zero level is about 5%. The mean signal-to-noise ratio of the final spectra is typically 10, 17 and 28 down to about 4000 Å, for Q 0058+019, Q 0453–423 and Q 2128–123 respectively.

3. Ionic column densities

Ionic column densities were derived from a least-squares technique using the *fitlyman* program (Fontana & Ballester 1995) in which Voigt profiles are convolved with the instrumental point spread function. The metal line profiles were fitted consistently assuming the same velocity for all the ions of a given component and a pure turbulent broadening. Whenever available, we used updated oscillator strength values (see Savage & Sembach 1996), or else the compilation by Morton (1991), except for the Fe II $\lambda\lambda 2344, 2374$ lines for which we used the laboratory measurements of Bergeson et al. (1996). The column densities of Mg I, Mg II, Si II, Ca II, Ti II, Cr II, Mn II, Fe II and Zn II were derived simultaneously and the results are shown in Table 2. In this Table, the standard deviations given in parentheses for unsaturated line components were also obtained with *fitlyman* from a simultaneous fit of all the lines observed in a given absorber; they should be realistic if the above assumed model is correct. In what follows, we adopt the Solar abundances given by Savage & Sembach (1996).

We now comment on the five individual systems of the sample with new observations.

3.1. Q 0058+019, $z_{\text{abs}} = 0.6125$

The total neutral hydrogen column density of this absorber was derived from the available HST FOS spectrum. We get $\log N(\text{H I}) = 20.14 \pm 0.09$. We adopted the column density estimated by (Pettini et al. 2000) for Fe II as it is based on the high signal-to-noise ratio detection of the weak, unsaturated Fe II $\lambda\lambda 2249, 2260$ lines in a Keck HIRES spectrum. Our Mn II measurement yields $[\text{Mn}/\text{Fe}] = -0.15 \pm 0.06$, which is slightly sub-solar. A 5σ detection of Ti II $\lambda 3384$ was reported by Churchill et al. (2000a) using new Keck HIRES data. The measured column density, $\log N(\text{Ti II}) = 12.53 \pm 0.08$ (Churchill, private communication), leads to an elemental ratio $[\text{Ti}/\text{Fe}] = -0.10 \pm 0.09$.

3.2. Q 0453–423, $z_{\text{abs}} = 0.7260$ and $z_{\text{abs}} = 1.1496$

As mentioned in Subsect. 2.1, the existence of an optically thick Lyman limit system at $z_{\text{abs}} \approx 2.3$ prevents a direct determination of the total H I column density of the $z_{\text{abs}} = 0.7260$ and 1.1496 strong metal-line systems. However, in both systems, $w_{\text{r}}(\text{Fe II } \lambda 2600)/w_{\text{r}}(\text{Mg II } \lambda 2796)$ is of order unity which, together with the strength of the Mg II lines, $w_{\text{r}}(\text{Mg II } \lambda 2796) > 1 \text{ \AA}$, implies that $N(\text{H I})$ is well in excess of a few 10^{19} cm^{-2} . Both absorbers should thus be moderate-DLA if not DLA systems (see Bergeron & Stasińska 1986; Rao & Turnshek 2000). For the system at $z_{\text{abs}} = 1.150$, the Fe II line profile is complex spanning about 550 km s^{-1} . A simultaneous least-square fit of the Fe II $\lambda\lambda 2249, 2260$ and Fe II $\lambda 2344$ profiles (the latter constraining the line parameters of the components 5 to 8; see Table 2) yields a *total* Fe II column density, $\log N(\text{Fe II}) = 15.18 \pm 0.08$, thus probably a high metallicity ($[\text{Fe}/\text{H}] > 0.5$). For the system at $z_{\text{abs}} = 0.726$, we measured $\log N(\text{Fe II}) = 14.54 \pm 0.04$. The Mn abundances relative to Fe derived using the method outlined in Sect. 4 are over-solar, $[\text{Mn}/\text{Fe}] = +0.12 \pm 0.09$ and $+0.34 \pm 0.20$ at $z_{\text{abs}} = 0.726$ and 1.150 respectively (see Table 3).

3.3. Q 1122–168, $z_{\text{abs}} = 0.6819$

This DLA system was recently studied by de la Varga et al. (2000) using ESO 3.6 m CASPEC and Keck HIRES data. From an HST FOS spectrum, these authors derived a total H I column density $\log N(\text{H I}) = 20.45 \pm 0.05$ from a fit of the Lyman- α and Lyman- β lines. In our very high signal-to-noise ratio UVES spectra, we measured accurate column densities for Fe II, Mn II and Ti II, and placed a stringent upper limit on the column density of Zn II (see Table 2). The Ca II lines are optically thin and their profile closely follows that of the Mg I $\lambda 2852$ line from -100 to $+200 \text{ km s}^{-1}$ (see Fig. 1). The Ca II over Mg I column density ratio is indeed essentially the same for all the components in which both species are detected, $\log(N(\text{Ca II})/N(\text{Mg I})) \simeq -0.28$, and is consistent with the prediction for warm gas with low depletion (e.g. Vladilo et al. 1997).

The Fe abundance derived from the weaker transitions of Fe II is $[\text{Fe}/\text{H}] = -1.40 \pm 0.05$. The non-detection of Zn II yields $[\text{Zn}/\text{Fe}] < +0.29$ and $< +0.39$ for components 3+4 and 9 respectively (see Table 2 and 3). This DLA system thus appears to be essentially dust-free (see also de la Varga et al. 2000). The Mn II column densities we derived for the components 3+4 and 9 lead to sub-solar elemental ratios, $[\text{Mn}/\text{Fe}] = -0.25 \pm 0.09$ and $[\text{Mn}/\text{Fe}] \leq -0.40 \pm 0.12$ respectively. Note that these values estimated for individual components are 0.3 to 0.4 dex higher than those integrated over the whole profile as given by de la Varga et al. (2000). This is due to a non-negligible contribution to the total Fe II column density of components detected in Fe II but not in Mn II. *This clearly demonstrates that systematic of this kind can dominate the abundance ratio variations in DLA systems.* The Ti abundance is derived from

a simultaneous fit of the Ti II $\lambda\lambda 3073, 3242, 3384$ lines. We get $[\text{Ti}/\text{Fe}] = +0.06 \pm 0.09$ and $[\text{Ti}/\text{Fe}] \leq -0.04 \pm 0.12$ for components 3 + 4 and 9 respectively.

3.4. Q 2128–123, $z_{\text{abs}} = 0.4298$

Our determination of the total H I column density from the HST FOS spectrum is $\log N(\text{H I}) = 19.37 \pm 0.08$. Although the Lyman- α line has damped wings, this value is lower than the threshold usually adopted for DLA systems ($\gtrsim 20.3$). Since $\log N(\text{H I}) \simeq 19.4$ corresponds to an optical depth at the Lyman limit $\tau_{\text{LL}} \simeq 150$, ionization corrections should be small (e.g. Viegas 1995). Furthermore, we concentrate our discussion below on relative abundances and these elements have negligible differential ionization corrections (see Vladilo et al. 2001).

In our ESO 3.6 m CASPEC spectrum, the line profiles from low-ionization species show two separated components spanning $\Delta V \simeq 75 \text{ km s}^{-1}$, the strongest component being located on the profile red side. A two velocity-component model was used to fit the Fe II and Mg II doublets and the Mg I line detected in the observed wavelength range, 3600–4100 Å (see Table 2). The velocity broadening of the main component is constrained by the Fe II $\lambda 2586$ profile, whereas that of the satellite component is determined from the strong Mg II doublet. Since the latter Fe II line may be saturated, we give only a lower limit on the column density: $\log N(\text{Fe II}) > 14.08$ in the main component. From the non-detection of the Mn II lines, we get $[\text{Mn}/\text{Fe}] < -0.03$ (see Table 3). From $\log N(\text{Ti II}) < 11.21$ (Churchill, private communication), we derive $[\text{Ti}/\text{Fe}] < -0.29$.

4. The DLA absorber sample

In order to investigate the abundance pattern of DLA systems and study dust depletion effects, we have built a sample of 24 DLA/moderate DLA (i.e. $\log N(\text{H I}) > 20.3/19.4 \leq \log N(\text{H I}) < 20.3$) systems at $0.3 < z_{\text{abs}} < 2.2$, all with measurements of the Mn II absorption lines. The sample, as shown in Table 3, includes seven DLA candidates selected on the basis of their large $0.6 \lesssim w_r(\text{Fe II } \lambda 2600)/w_r(\text{Mg II } \lambda 2796) \lesssim 1.0$ equivalent width ratio. We give the measured abundances of Si, Ti, Cr, Mn and Zn relative to Fe. The previously analyzed Mn samples are those of Lu et al. (1996), which includes seven Mn II systems at $0.86 \leq z_{\text{abs}} \leq 2.14$ of which three are associated with DLA candidates, and Pettini et al. (2000), which includes six Mn II systems at $0.61 \leq z_{\text{abs}} \leq 1.42$ of which one is in common with those of Lu et al. In our sample, there are nine Ti II detections and three upper limits for systems at $0.43 \leq z_{\text{abs}} \leq 1.96$. The Ti abundance measurements in the DLA systems toward Q 0058+019, Q 0454+039, Q 1622+238 and Q 2128–123 were kindly made available to us by C. W. Churchill. They were derived from Keck HIRES spectra obtained for another project (Churchill et al. 2000a,b). The sample of six

Ti II absorbers detected by Prochaska et al. (2001) covers a somewhat higher redshift range, $1.78 \leq z_{\text{abs}} \leq 2.10$.

The relative abundances in the gaseous phase of DLA systems are usually determined from column densities integrated over the entire absorption profiles. This procedure leads to unbiased results only when all the components observed in the profiles of strong absorption lines are also detected in weaker transition lines. However, the optical depth of most of the Fe II lines are larger than those of the Mn II, Ti II, Cr II and Zn II transitions. As the overall profiles of the weaker transitions are usually less extended than those of the Fe II lines, the above procedure tends to overestimate the column density of Fe II as compared to other species. For this reason, we have used a different approach. After performing the Voigt profile fits of all of the absorption profiles, we summed up only the column densities of the components detected in at least one of the Mn II, Ti II, Cr II or Zn II ions (note that these ions, when observed, are usually detected at the same time). These components correspond most often to the strongest part of the profiles.

Our procedure tends to minimize the impact of limitations due to finite signal-to-noise ratios whereas the standard procedure can lead to underestimate the abundances of rare elements relative to Fe by -0.1 up to -0.3 dex (as is the case for the DLA system toward Q 1122–168). For DLA systems at intermediate redshifts, we also applied this procedure to all the data taken from the literature when a detailed modeling was available (see Table 3). However, for the estimate of the absolute $[\text{Fe}/\text{H}]$ abundances, we include all the components of Fe II for comparison with previous studies.

5. Observed abundance pattern

We present in Table 3 the abundance of Fe and elemental abundance ratios relative to Fe for our sample. From the analysis of a DLA sample at intermediate redshift, Pettini et al. (1999) showed that there is no significant cosmic evolution of DLA metallicity ($[\text{Zn}/\text{H}]$) in our redshift range, $0.3 < z_{\text{abs}} < 2.2$. The elemental abundance ratios presented in Fig. 2 and Table 4 do not exhibit any significant evolution with redshift either. The scatter of these abundance ratios is very small for $[\text{Cr}/\text{Fe}]$ and about 1 dex for $[\text{Mn}/\text{Fe}]$ and $[\text{Zn}/\text{Fe}]$.

We examine below the observed abundance patterns to identify the elements which would clearly help separating the effects of star-formation history and depletion of refractory elements onto dust grains.

5.1. Zn and Cr

In DLA systems at $0.3 < z_{\text{abs}} < 2.2$, Zn and Cr are both observed to be overabundant relative to Fe (see Fig. 2). The spread in $[\text{Zn}/\text{Fe}]$ ranges from a solar ratio up to overabundances of about $+0.8$, with a mean of about $+0.5$ (see Table 4). It is unclear whether an overabundance of

Zn relative to Fe can be explained by stellar nucleosynthesis models. The channels of Zn production in massive stars are not yet fully understood and the predictions of standard nucleosynthesis models lie at least a factor of 2 below the observed stellar abundances of Zn (Timmes et al. 1995; Thielemann et al. 1996; however see Umeda & Nomoto 2002). Additional processes might produce important amounts of Zn, such as axi-symmetrically deformed explosions in type II supernovae (Nagataki 1999) and p -processing in the neutrino-driven wind following the supernovae explosions (Hoffman et al. 1996), but quantitative results depend on uncertain parameters. Moreover, in Galactic thin disk stars the observed abundance of Zn follows that of Fe with $[\text{Zn}/\text{Fe}] = +0.04 \pm 0.10$ and in Galactic thick disk and halo stars the observed $[\text{Zn}/\text{Fe}]$ ratio is in the range (0,+0.2) (see Prochaska et al. 2000, and references therein). Finally, in the Galactic ISM, Zn is mostly undepleted even in dust-rich regions.

We thus infer that, except maybe for elemental ratios $[\text{Zn}/\text{Fe}]_{\text{obs}} \lesssim +0.2$ (see also Sect. 6), dust depletion should be the main effect governing the observed $[\text{Zn}/\text{Fe}]$ abundance pattern of DLA systems.

In DLA absorbers, the observed $[\text{Cr}/\text{Fe}]$ ratio shows very little scatter whatever the metallicity (see Table 3), z_{abs} (see Fig. 2) or $[\text{Zn}/\text{Fe}]$ (see Fig. 3). The overabundance of Cr relative to Fe ($\sim +0.15$) was already noted (Lu et al. 1996; Prochaska & Wolfe 1999). It cannot be accounted for solely by dust depletion since it is present even in systems with only small amounts of dust ($0 \lesssim [\text{Zn}/\text{Fe}] < 0.3$) or of low metallicity ($[\text{Zn}/\text{H}] < -1$). Moreover, Cr and Fe are depleted onto dust grains by fairly similar amounts in the warm ISM of the Galaxy, $[\text{Cr}/\text{Fe}]_{\text{ISM}} \simeq +0.13$ (see Savage & Sembach 1996) and the ISM of the SMC (see Table 4). However, this elemental ratio is larger in DLA absorbers than in Galactic stars by a factor of about +0.15 dex and close to those observed in the stars of the SMC (see Table 4). In current chemical evolution models, the abundance of Cr closely follows that of Fe for a wide range of metallicities (e.g. Timmes et al. 1995; Goswami & Prantzos 2000). These models reproduce the trend observed in Galactic stars but not the SMC value. Therefore, in DLA absorbers dust depletion effects could be important, as well as nucleosynthesis ones as for SMC stars.

5.2. Mn, Si and Ti

In DLA absorbers, the abundance of Mn relative to Fe spans a larger range than previously found from smaller samples. For a substantial fraction of our sample, we get $-0.5 \lesssim [\text{Mn}/\text{Fe}] \lesssim 0$, but there are also five systems at $z_{\text{abs}} < 1.4$ with $[\text{Mn}/\text{Fe}] > 0$ (see Fig. 2). Of the latter, only one is a confirmed DLA absorber with $\log N(\text{H I}) > 20.3$. As can be seen in Table 4, the mean abundance of Mn, an odd- Z Fe-peak element, in DLA systems is close to that observed in Galactic metal-poor halo stars (McWilliam et al. 1995; Ryan et al. 1996) and the cases with $[\text{Mn}/\text{Fe}] \sim 0$ are similar to those of SMC

stars. The dust depletion level of Mn is about the same as that of Fe in Galactic warm halo clouds and slightly lower in Galactic warm disk clouds (Savage & Sembach 1996). From the spread of values of $[\text{Mn}/\text{Fe}]$ in DLA absorbers together with the small relative ionization correction factors for these elements (as well as for Ti: see e.g. Vladilo et al. 2001), we thus infer that both nucleosynthesis and dust depletion effects are needed to account for this elemental ratio.

The abundances of the two α -elements Si and Ti are larger than solar in DLA absorbers, with a few cases slightly sub-solar for Ti (see Fig. 2). These elements are also overabundant in Galactic halo and SMC stars (see Table 4). The overabundance of Si can be a consequence of nucleosynthesis effects (Lu et al. 1996; Pettini et al. 2000) since in Galactic chemical evolution models the abundance of α -elements is enhanced as compared to solar for metallicities $-2 \lesssim [\text{Fe}/\text{H}] \lesssim -1$ (e.g. Timmes et al. 1995; McWilliam 1997). However, it is also consistent with a dust depletion pattern similar to that observed in Galactic warm disk and halo clouds (see Sect. 6). As Ti is observed to be more depleted onto dust grains than Fe in Galactic warm halo clouds, nucleosynthesis effects are most probably required to account for the observed over-solar $[\text{Ti}/\text{Fe}]$ ratios of DLA systems, and this, whatever the dust content. However, dust depletion could be the dominant factor for the few cases with observed, sub-solar $[\text{Ti}/\text{Fe}]$ ratio.

6. Depletion sequences

6.1. Method

When a uniform depletion fraction is assumed, the intrinsic abundances are simply given by:

$$10^{[\frac{X}{Zn}]_{\text{dc}}} = 10^{[\frac{X}{Zn}]_{\text{obs}}} \cdot 10^{[\frac{Zn}{Cr}]_{\text{obs}}}, \quad (1)$$

This depletion correction follows the observed composition of the gaseous phase, thus does not change the relative abundances. It should be used only for low depletion factors, $[\text{Zn}/\text{Fe}]_{\text{obs}} \lesssim +0.3$, i.e. for only a small fraction of our sample.

A simple method which takes into account the dust composition was developed by Vladilo (1998). Various depletion patterns can be used with different fractions, f_X , of an element X locked onto dust grains. From Vladilo's Eqs. (17) and (18), introducing explicitly in Eq. (18) the intrinsic $[\text{Zn}/\text{Fe}]$ elemental ratio to allow for non-solar values, we derive the following general relation:

$$10^{[\frac{X}{Fe}]_{\text{obs}}} = \frac{10^{[\frac{X}{Fe}]_{\text{dc}}} - \frac{\tilde{k}}{\tilde{Z}} f_X \cdot 10^{[\frac{Zn}{Fe}]_{\text{dc}}}}{1 - \frac{\tilde{k}}{\tilde{Z}} f_{\text{Fe}} \cdot 10^{[\frac{Zn}{Fe}]_{\text{dc}}}}, \quad (2)$$

where the label “dc” refers to intrinsic (dust corrected) elemental ratios, and \tilde{k}/\tilde{Z} is the dust-to-metal ratio normalized to the Galactic value.

To compute a “depletion sequence”, $[\text{X}/\text{Fe}]_{\text{obs}}$ versus $[\text{Zn}/\text{Fe}]_{\text{obs}}$, we need to assume a value for $[\text{Zn}/\text{Fe}]_{\text{dc}}$. Since in Galactic stars of low metallicity and in SMC stars this

ratio is observed to be slightly over-solar, $0 \lesssim [\text{Zn}/\text{Fe}] \lesssim +0.2$ (see Table 4), we discuss in Sect. 7 the effect of a slight overabundance of Zn relative to Fe on the dust depletion correction.

6.2. Results

We present in Fig. 3 the observed abundance ratios of Si, Ti, Cr and Mn relative to Fe versus $[\text{Zn}/\text{Fe}]_{\text{obs}}$ together with depletion sequences for various depletion patterns, namely those of Galactic cold disk clouds, Galactic warm disk and Galactic warm halo clouds as provided by Welty et al. (1999). The observations show a correlation between $[\text{Si}/\text{Fe}]_{\text{obs}}$ and $[\text{Zn}/\text{Fe}]_{\text{obs}}$, detected at the 2.9σ significance level using a Kendall rank correlation test. A similar trend is present in the higher redshift sample analyzed by Prochaska & Wolfe (1999). Such a correlation is fully consistent with a dust depletion sequence. The best agreement between model and observations is obtained for the Galactic warm disk and warm halo cloud patterns. These patterns are similar to those observed in the ISM of the SMC (Welty et al. 2001). The Galactic warm halo cloud pattern is also close to that observed in the Magellanic Bridge (Lehner et al. 2001) where the overall metallicity may be even lower than in the SMC. In addition, the data allows for intrinsic elemental ratios slightly over-solar, $0 < [\text{Si}/\text{Fe}]_{\text{dc}} < +0.2$. A good depletion sequence fit is then also obtained for $[\text{Si}/\text{Fe}]_{\text{dc}} \simeq [\text{Zn}/\text{Fe}]_{\text{dc}} = +0.1$. We thus conclude that, although some nucleosynthesis effects could be present (see Sect. 7), the variations of the observed $[\text{Si}/\text{Fe}]$ elemental ratio should mainly be due to dust depletion.

Being fairly constant down to low depletion levels, the $[\text{Cr}/\text{Fe}]_{\text{obs}}$ ratio is not well fitted by a depletion sequence, although a large fraction of the data points are roughly consistent with dust depletion if an intrinsic overabundance of Cr relative to Fe of +0.1 dex is considered (see Fig. 3). This small overabundance is not observed in Galactic metal-poor stars (McWilliam et al. 1995), whereas it is present in both the ISM and the stars of the SMC. Although current chemical evolution models reproduce satisfactorily a constant $[\text{Cr}/\text{Fe}] \approx 0$ (see e.g. Timmes et al. 1995; Goswami & Prantzos 2000), they do not account for a slight overabundance of Cr relative to Fe.

The $[\text{Mn}/\text{Fe}]_{\text{obs}}$ ratios cannot be fitted by any dust depletion sequence (see Fig. 3), even if non-solar values are considered for the intrinsic $[\text{Mn}/\text{Fe}]_{\text{dc}}$ ratio. The observed values can only be recovered if one assumes possible variations of this intrinsic elemental ratio in the range -0.3 to $+0.1$ dex. For the 17 DLA systems with both Mn and Zn measurements, there is a trend for an increase of $[\text{Mn}/\text{Fe}]_{\text{obs}}$ with increasing $[\text{Zn}/\text{Fe}]_{\text{obs}}$, detected at the 3.2σ significance level using a Kendall rank correlation test (limits are taken into account as true detections). This trend may be the consequence of a relation between depletion level and metallicity. To test this suggestion, we investigate the variations of $[\text{Zn}/\text{Fe}]_{\text{obs}}$ and $[\text{Si}/\text{Fe}]_{\text{obs}}$ ver-

sus $[\text{Zn}/\text{H}]_{\text{obs}}$, Si being much less depleted than Mn, Cr and Fe in the Galactic ISM. They are presented in the upper panels of Fig. 4. For these two elemental ratios, there is a marginal correlation with metallicity, present only for both at the 1.7σ significance level. To confirm this possible correlation between depletion level and metallicity would require larger samples, in particular an extension at low metallicity, $-2.0 \lesssim [\text{Zn}/\text{H}]_{\text{obs}} \lesssim -1.5$. Whereas $[\text{Cr}/\text{Fe}]_{\text{obs}}$ does not show any variation with metallicity there is a clear increase of $[\text{Mn}/\text{Fe}]_{\text{obs}}$ with increasing metallicity detected at the 2.6σ significance level. This correlation suggests for the first time that, on average, the intrinsic $[\text{Mn}/\text{Fe}]$ ratio gets more sub-solar toward lower metallicity, a trend which is compatible with the pattern observed in Galactic halo stars (see Table 4).

Although the number of Ti measurements is small, the variation of $[\text{Ti}/\text{Fe}]_{\text{obs}}$ with $[\text{Zn}/\text{Fe}]_{\text{obs}}$ cannot be fitted either by a single dust depletion sequence. As for Mn, this suggests a variation of the intrinsic $[\text{Ti}/\text{Fe}]_{\text{dc}}$ ratio. Since Ti is more depleted onto dust grains than Fe, the positive values of $[\text{Ti}/\text{Fe}]_{\text{obs}}$ observed in most cases would imply, as for the other α -element in our study, Si, an over-solar, intrinsic $[\text{Ti}/\text{Fe}]_{\text{dc}}$ elemental ratio (see below).

7. Discussion

We now discuss the intrinsic elemental ratios derived from Eq. (2) for the 24 DLA absorbers of our sample at $0.3 < z_{\text{abs}} < 2.2$. Since the depletion pattern of Galactic cold disk clouds does not fit the correlation between $[\text{Si}/\text{Fe}]_{\text{obs}}$ and $[\text{Zn}/\text{Fe}]_{\text{obs}}$ for an intrinsic elemental ratio $[\text{Si}/\text{Fe}]_{\text{dc}} < +0.1$, we use the dust depletion patterns of either Galactic warm disk or warm halo clouds. We present in Fig. 5 the dust-corrected abundance ratios versus metallicity, as given by $[\text{Fe}/\text{H}]_{\text{dc}}$. As most of the DLA absorbers of our sample have sub-solar abundances, we assume a value for $[\text{Zn}/\text{Fe}]_{\text{dc}}$ equal to that observed in Galactic metal-poor and SMC stars (see Table 4), i.e. $[\text{Zn}/\text{Fe}]_{\text{dc}} = +0.1$. This implies $[\text{Si}/\text{Zn}]_{\text{dc}} = [\text{Cr}/\text{Zn}]_{\text{dc}} = 0$ (see Fig. 3 and Subsect. 6.2). If we had assumed a solar $[\text{Zn}/\text{Fe}]_{\text{dc}}$ ratio, the trends discussed below would be similar and there would be only very small shifts (~ -0.05 dex) in the absolute values of the dust-corrected abundance ratios.

As discussed in Subsect. 6.2, the importance of nucleosynthesis effects is already revealed by the different behaviours of the observed abundances of Mn and Cr relative to Fe. The fractions of these two elements locked onto dust grains are similar (and also close to that for Fe) and they have comparable solar abundances relative to Fe. However, whereas the $[\text{Cr}/\text{Fe}]_{\text{obs}}$ ratio is fairly constant whatever the metallicity, the correlation observed between $[\text{Mn}/\text{Fe}]_{\text{obs}}$ and metallicity (Fig. 4) implies an increase of the intrinsic abundance of Mn relative to Fe with metallicity.

To compare the intrinsic abundance patterns observed in DLA systems with those of Galactic and SMC stars, we also give in Fig. 5 the relation between the abundance

ratios and metallicity observed in Galactic thin disk and halo stars (from the compilation of values by Prochaska et al. 2000) as well as the values for SMC stars (from the appendix of Welty et al. 1997). For the trend shown for Mn in Galactic stars, we took into account the hyper-fine structure splitting effects of the Mn I lines (Prochaska & McWilliam 2000) which leads to a slightly higher $[\text{Mn}/\text{Fe}]$ mean ratio, now equal to -0.05 at $[\text{Fe}/\text{H}] \gtrsim -0.5$.

We note that the intrinsic abundances of the two α -elements, Si and Ti, relative to Fe show a similar trend versus metallicity, although the dust depletion pattern used to determine these intrinsic elemental ratios was derived from the correlation present between $[\text{Si}/\text{Fe}]_{\text{obs}}$ and $[\text{Zn}/\text{Fe}]_{\text{obs}}$ only. This strengthens our choice of warm dust depletion patterns and dust depletion correction method.

For the few DLA absorbers of fairly high metallicity, $[\text{Fe}/\text{H}]_{\text{dc}} \gtrsim -0.5$, all four elemental ratios: $[\text{Si}/\text{Fe}]_{\text{dc}}$, $[\text{Cr}/\text{Fe}]_{\text{dc}}$, $[\text{Ti}/\text{Fe}]_{\text{dc}}$ and $[\text{Mn}/\text{Fe}]_{\text{dc}}$ follow the trends present in Galactic stars and, at $[\text{Fe}/\text{H}]_{\text{dc}} \simeq 0$, their abundances relative to Fe are about equal to the solar values. The chemical evolution of these DLA systems appears to be similar to that of our Galaxy.

At the metallicity of the SMC, $[\text{Fe}/\text{H}] \approx -0.6$, the DLA dust-corrected abundances of Si, Ti and Cr relative to Fe, and in a lesser extent that of Mn, are close to those of SMC stars (see Fig. 5 and Table 4) with $[\text{Si}/\text{Fe}]_{\text{dc}} \sim [\text{Ti}/\text{Fe}]_{\text{dc}} \sim [\text{Cr}/\text{Fe}]_{\text{dc}} \sim +0.1$ and $[\text{Mn}/\text{Fe}]_{\text{dc}} \sim 0$.

However, at lower metallicity, $[\text{Fe}/\text{H}]_{\text{dc}} < -0.6$, for a substantial fraction of DLA absorbers the intrinsic abundances of Si, Ti and Mn relative to Fe are closer to the solar values than for Galactic stars and show little variation with decreasing metallicity. The evolution of $[\text{Mn}/\text{Fe}]_{\text{dc}}$ with metallicity is well accounted for by the odd-even effects for the Fe-peak elements using metallicity dependent yields (for Galactic models see e.g. Timmes et al. 1995; Goswami & Prantzos 2000). Furthermore, the systems with $[\text{Si}/\text{Fe}]_{\text{dc}} \sim [\text{Ti}/\text{Fe}]_{\text{dc}} \lesssim +0.10$ (resp. $> +0.10$) are indeed also those with $[\text{Mn}/\text{Fe}]_{\text{dc}} > -0.15$ (resp. < -0.15), i.e. there is an anti-correlation between $[\text{Mn}/\text{Fe}]_{\text{dc}}$ and $[\text{Si}/\text{Fe}]_{\text{dc}}$ or $[\text{Ti}/\text{Fe}]_{\text{dc}}$. This strongly suggests that the contribution of type Ia supernovae to the chemical enrichment of the metal-poor DLA systems with $[\text{Si}/\text{Fe}]_{\text{dc}} \sim [\text{Ti}/\text{Fe}]_{\text{dc}} \sim +0.1$ and $[\text{Mn}/\text{Fe}]_{\text{dc}} \sim -0.1$ is larger than for Galactic stars of comparable metallicity. This conclusion is consistent with the interpretations of Matteucci et al. (1997) and Legrand et al. (2000) based on other abundance ratios, which favor at least for some DLA absorbers an episodic or slow star-formation scenario. If they have experienced instantaneous starbursts, these DLA absorbers should thus be older than 50 Myr (see Matteucci & Recchi 2001). Since there is a wide spread of galactic morphological types among the identified DLA absorbers (Le Brun et al. 1997), the metal-poor DLA absorbers with abundance ratios fairly close to the solar values could indeed trace the H I-rich dwarf galaxy population.

Among the goals for future work, we identify the extension of DLA samples at low $[\text{Zn}/\text{H}]$ to test the possible

correlation between depletion level and metallicity, and observations of S and Zn in the same DLA systems to confirm the lack of depletion for Zn and distinguish further between different star-formation histories from a comparison of $[\text{S}/\text{Fe}]$ or $[\text{Zn}]$ in DLA absorbers and in Galactic/SMC stars.

Acknowledgements. We are grateful to C. W. Churchill for making available to us unpublished data on the Ti abundances of four DLA systems and N. Prantzos for fruitful discussion. We thank R. Srianand for the reduction of the echelle spectrum of Q0453–423. CL acknowledges support from an ESO post-doctoral fellowship. This work was supported by the European Community Research and Training Network: "The Physics of the Intergalactic Medium".

References

- Ballester, P., Modigliani, A., Boitquin, O., et al. 2000, *The Messenger*, 101, 31
- Bergeron, J. & D’Odorico, S. 1986, *MNRAS*, 220, 833
- Bergeron, J. & Stasińska, G. 1986, *A&A*, 169, 1
- Bergeson, S. D., Mullman, K. L., Wickliffe, M. E., et al. 1996, *ApJ*, 464, 1044
- Blades, J. C., Hunstead, R. W., Murdoch, H. S., & Pettini, M. 1982, *MNRAS*, 200, 1091
- . 1985, *ApJ*, 288, 580
- Boissé, P., Le Brun, V., Bergeron, J., & Deharveng, J.-M. 1998, *A&A*, 333, 841
- Churchill, C. W., Mellon, R. R., Charlton, J. C., et al. 2000a, *ApJS*, 130, 91
- . 2000b, *ApJ*, 543, 577
- Cohen, R. D., Barlow, T. A., Beaver, E. A., et al. 1994, *ApJ*, 421, 453
- de la Varga, A., Reimers, D., Tytler, D., Barlow, T. A., & Burles, S. 2000, *A&A*, 363, 69
- Fontana, A. & Ballester, P. 1995, *The Messenger*, 80, 37
- Goswami, A. & Prantzos, N. 2000, *A&A*, 359, 191
- Hoffman, R. D., Woosley, S. E., Fuller, G. M., & Meyer, B. S. 1996, *ApJ*, 460, 478
- Kulkarni, V. P., Fall, S. M., & Truran, J. W. 1997, *ApJ*, 484, L7
- Lanzetta, K. M. & Bowen, D. V. 1992, *ApJ*, 391, 48
- Le Brun, V., Bergeron, J., Boissé, P., & Deharveng, J.-M. 1997, *A&A*, 321, 733
- Ledoux, C., Petitjean, P., Bergeron, J., Wampler, E. J., & Srianand, R. 1998, *A&A*, 337, 51
- Ledoux, C., Srianand, R., & Petitjean, P. 2002, *MNRAS*, submitted
- Legrand, F., Kunth, D., Roy, J.-R., Mas-Hesse, J. M., & Walsh, J. R. 2000, *A&A*, 355, 891
- Lehner, N., Sembach, K. R., Dufton, P. L., Rolleston, W. R. J., & Keenan, F. P. 2001, *ApJ*, 551, 781
- Lopez, S., Reimers, D., Rauch, M., Sargent, W. L. W., & Smette, A. 1999, *ApJ*, 513, 598
- Lu, L., Sargent, W. L. W., Barlow, T. A., Churchill, C. W., & Vogt, S. S. 1996, *ApJS*, 107, 475
- Lu, L., Savage, B. D., Tripp, T. M., & Meyer, D. M. 1995, *ApJ*, 447, 597

- Matteucci, F., Molaro, P., & Vladilo, G. 1997, *A&A*, 321, 45
- Matteucci, F. & Recchi, S. 2001, *ApJ*, 558, 351
- McWilliam, A. 1997, *ARA&A*, 35, 503
- McWilliam, A., Preston, G. W., Sneden, C., & Searle, L. 1995, *AJ*, 109, 2757
- Meyer, D. M., Lanzetta, K. M., & Wolfe, A. M. 1995, *ApJ*, 451, L13
- Meyer, D. M. & York, D. G. 1992, *ApJ*, 399, L121
- Morton, D. C. 1991, *ApJS*, 77, 119
- Nagataki, S. 1999, *ApJ*, 511, 341
- Petitjean, P. & Bergeron, J. 1994, *A&A*, 283, 759
- Petitjean, P., Srianand, R., & Ledoux, C. 2002, *MNRAS*, in press, astro-ph/0201477
- Pettini, M., Ellison, S. L., Steidel, C. C., & Bowen, D. V. 1999, *ApJ*, 510, 576
- Pettini, M., Ellison, S. L., Steidel, C. C., Shapley, A. E., & Bowen, D. V. 2000, *ApJ*, 532, 65
- Pettini, M., King, D. L., Smith, L. J., & Hunstead, R. W. 1997a, *ApJ*, 478, 536
- Pettini, M., Smith, L. J., Hunstead, R. W., & King, D. L. 1994, *ApJ*, 426, 79
- Pettini, M., Smith, L. J., King, D. L., & Hunstead, R. W. 1997b, *ApJ*, 486, 665
- Prochaska, J. X. & McWilliam, A. 2000, *ApJ*, 537, L57
- Prochaska, J. X., Naumov, S. O., Carney, B. W., McWilliam, A., & Wolfe, A. M. 2000, *AJ*, 120, 2513
- Prochaska, J. X. & Wolfe, A. M. 1997a, *ApJ*, 487, 73
- . 1997b, *ApJ*, 474, 140
- . 1999, *ApJS*, 121, 369
- Prochaska, J. X., Wolfe, A. M., Tytler, D., et al. 2001, *ApJS*, 137, 21
- Rao, S. M. & Turnshek, D. A. 2000, *ApJS*, 130, 1
- Ryan, S. G., Norris, J. E., & Beers, T. C. 1996, *ApJ*, 471, 254
- Savage, B. D. & Sembach, K. R. 1996, *ARA&A*, 34, 279
- Steidel, C. C., Dickinson, M., Meyer, D. M., Adelberger, K. L., & Sembach, K. R. 1997, *ApJ*, 480, 568
- Thielemann, F.-K., Nomoto, K., & Hashimoto, M. 1996, *ApJ*, 460, 408
- Timmes, F. X., Woosley, S. E., & Weaver, T. A. 1995, *ApJS*, 98, 617
- Umeda, H. & Nomoto, K. 2002, *ApJ*, 565, 385
- Véron-Cetty, M.-P. & Véron, P. 2001, *A&A*, 374, 92
- Viegas, S. M. 1995, *MNRAS*, 276, 268
- Vladilo, G. 1998, *ApJ*, 493, 583
- Vladilo, G., Centurión, M., Bonifacio, P., & Howk, J. C. 2001, *ApJ*, 557, 1007
- Vladilo, G., Centurión, M., Falomo, R., & Molaro, P. 1997, *A&A*, 327, 47
- Welty, D. E., Hobbs, L. M., Lauroesch, J. T., et al. 1999, *ApJS*, 124, 465
- Welty, D. E., Lauroesch, J. T., Blades, J. C., Hobbs, L. M., & York, D. G. 1997, *ApJ*, 489, 672
- . 2001, *ApJ*, 554, L75
- Wolfe, A. M., Turnshek, D. A., Smith, H. E., & Cohen, R. D. 1986, *ApJS*, 61, 249

Table 1. Observational data:

Quasar	mag ^a	z_{em}^{a}	Telescope	Instrument	Wavelength range (Å)	Resolution FWHM (Å)	Exposure time (s)	Comment
0058+019	17.16 (V)	1.959	ESO 3.6 m	CASPEC	3510–4797	0.16	21600	
			HST	FOS	1572–2311	0.84	1590	G190H
0453–423	17.06 (V)	2.661	ESO 3.6 m	CASPEC	3680–5096	0.16	16200	
			HST	FOS	1572–2311	0.84	1700	G190H
			HST	FOS	2223–3277	1.19	2440	G270H
1122–168	16.20 (R)	2.400	VLT-UT2	UVES	3350–3875	0.10	26400	Dic #1
			VLT-UT2	UVES	4780–6815 ^b	0.10	26400	Dic #1
			VLT-UT2	UVES	3875–4780	0.10	27000	
2128–123	16.11 (V)	0.501	ESO 3.6 m	CASPEC	3510–4797	0.16	21600	
			HST	FOS	1572–2311	0.84	5221	G190H

^a Apparent magnitudes and emission redshifts are from Véron-Cetty & Véron (2001).

^b The small 5765–5837 Å interval was not covered due to the gap between red CCDs.

Table 2. Model fit parameters for individual components:

n	z_{abs}	ΔV km s ⁻¹	Ion	b (σ_b) km s ⁻¹	$\log N(\sigma_{\log N})$	n	z_{abs}	ΔV km s ⁻¹	Ion	b (σ_b) km s ⁻¹	$\log N(\sigma_{\log N})$
Q 0058+019						Q 1122–168					
1	0.612102	-51	Mg I	7.0 (....)	<11.00 ^a	1	0.681309	-99	Mg I	4.0 (0.2)	10.75(0.07)
			Mg II		12.73(0.05)				Mg II		12.77(0.02)
			Mn II		<11.98 ^a				Fe II		12.39(0.02)
			Fe II		12.79(0.07)	2	0.681415	-80	Mg I	8.6 (1.0)	10.38(0.20)
2	0.612377	0	Mg I	13.0 (....)	12.35(0.05)				Mg II		11.88(0.04)
			Mg II		>15.98				Fe II		11.45(0.13)
			Mn II		12.88(0.04)	3	0.681862	0	Mg I	3.4 (0.1)	10.82(0.06)
			Fe II		15.11(0.08)				Ca II		10.69(0.14)
3	0.612519	+26	Mg I	13.0 (....)	12.13(0.06)				Ti II		11.22(0.08)
			Mg II		>14.18				Mn II		11.52(0.07)
			Mn II		12.65(0.06)				Fe II		13.86(0.03)
			Fe II		14.98(0.09)				Zn II		<11.26 ^a
4	0.612719	+64	Mg I	13.0 (....)	11.81(0.07)	4	0.681919	+10	Mg I	8.2 (0.3)	11.01(0.05)
			Mg II		>15.01				Ca II		10.59(0.23)
			Mn II		12.10(0.16)				Ti II		11.39(0.07)
			Fe II		13.99(0.06)				Mn II		11.66(0.07)
5	0.612973	+111	Mg I	11.2 (0.7)	11.46(0.13)				Fe II		13.79(0.02)
			Mg II		>13.89				Zn II		<11.26 ^a
			Mn II		<11.98 ^a	5	0.682025	+29	Mg I	8.9 (0.4)	10.91(0.07)
			Fe II		13.75(0.04)				Ca II		10.46(0.30)
Q 0453–423									Fe II		13.67(0.02)
1	0.725853	-33	Mg I	26.5 (0.8)	12.16(0.04)	6	0.682202	+61	Mg I	17.8 (0.6)	11.54(0.02)
			Mg II		>13.97				Ca II		11.16(0.08)
			Mn II		12.34(0.06)				Ti II		≤11.30(0.12)
			Fe II		14.27(0.03)				Mn II		≤11.76(0.07)
2	0.726043	0	Mg I	16.2 (1.0)	12.21(0.03)				Fe II		13.91(0.01)
			Mg II		>13.53	7	0.682353	+88	Mg I	7.3 (0.4)	10.90(0.07)
			Mn II		12.22(0.07)				Ca II		10.61(0.20)
			Fe II		14.01(0.05)				Fe II		13.31(0.03)
3	0.726280	+41	Mg I	23.4 (0.9)	11.56(0.09)	8	0.682459	+106	Mg I	11.7 (1.6)	10.79(0.10)
			Mg II		>13.57				Ca II		10.83(0.15)
			Mn II		11.95(0.11)				Fe II		13.07(0.05)
			Fe II		13.75(0.02)	9	0.682560	+125	Mg I	7.7 (0.1)	11.69(0.01)
1	1.148673	-129	Fe II	30.0 (....)	13.95(0.09)				Ca II		11.41(0.04)
2	1.149060	-75	Si II	30.0 (....)	≤14.72(0.13)				Ti II		≤11.11(0.12)
			Ti II		<12.62 ^a				Mn II		≤11.35(0.12)
			Cr II		≤12.98(0.08)				Fe II		13.73(0.01)
			Fe II		14.55(0.08)				Zn II		<11.26 ^a
			Zn II		≤12.01(0.21)	10	0.682693	+148	Mg I	10.6 (0.3)	11.30(0.03)
3	1.149598	0	Si II	23.5 (3.3)	≤14.97(0.07)				Ca II		10.92(0.11)
			Ti II		<12.62 ^a				Fe II		12.98(0.01)
			Cr II		≤12.85(0.10)	11	0.682928	+190	Mg I	5.2 (0.2)	10.77(0.07)
			Fe II		14.83(0.06)				Ca II		10.73(0.13)
			Zn II		≤12.27(0.11)				Fe II		12.81(0.01)
4	1.150024	+59	Fe II	25.9 (3.1)	14.28(0.08)	Q 2128–123					
5	1.150482	+123	Fe II	16.3 (1.4)	13.55(0.03)	1	0.429637	-37	Mg I	11.2 (0.9)	<10.88 ^a
6	1.150980	+193	Si II	30.0 (....)	≤14.71(0.12)				Mg II		12.46(0.02)
			Fe II		13.71(0.03)				Mn II		<11.77 ^a
7	1.151371	+247	Si II	30.0 (....)	<14.47 ^a				Fe II		12.66(0.05)
			Fe II		13.67(0.03)	2	0.429815	0	Mg I	8.3 (0.4)	12.18(0.02)
8	1.151953	+329	Si II	20.3 (0.9)	≤15.69(0.02)				Mg II		>14.11
			Fe II		13.88(0.02)				Mn II		≤12.07(0.08)
									Fe II		>14.08

^a 3 σ upper limits.

Table 3. Observed abundance ratios for DLA systems at $0.3 < z_{\text{abs}} < 2.2$:

Quasar	z_{abs}	$\log N(\text{H I})$	$[\text{Fe}/\text{H}]^2$	$[\text{Zn}/\text{Fe}]$	$[\text{Cr}/\text{Fe}]$	$[\text{Mn}/\text{Fe}]$	$[\text{Si}/\text{Fe}]$	$[\text{Ti}/\text{Fe}]$	Refs.
0058+019	0.612	20.14(0.09)	-0.41(0.10)	+0.46(0.13)	+0.19(0.08)	-0.15(0.06)	...	-0.10(0.09)	*,a,b
0118-272	0.558	... ¹	-1.06	+0.36(0.07)	...	+0.50(0.07)	c
0215+015	1.345	19.57(0.20)	-0.80(0.23)	+0.30(0.17)	>+0.32	...	d,e
0216+080	1.769	20.00(0.18)	-0.98(0.20)	<+0.67	<+0.36	-0.07(0.14)	+0.32(0.14)	...	f
0302-223	1.009	20.36(0.11)	-1.20(0.12)	+0.65(0.06)	+0.25(0.06)	-0.11(0.06)	+0.48(0.06)	...	a
0449-134	1.267	... ¹	-0.38	-0.28(0.04)	f
0450-132	1.174	... ¹	-0.39	<+0.54	+0.15(0.14)	-0.22(0.10)	f
0453-423	0.726	... ¹	-0.97	+0.12(0.09)	*
0453-423	1.150	... ¹	-0.33	≤+0.31	≤+0.00	+0.34(0.20)	≤+0.11	<+0.59	*,g
0454+039	0.860	20.69(0.07)	-1.03(0.09)	+0.02(0.08)	+0.15(0.06)	-0.28(0.06)	+0.24(0.08)	+0.15(0.05)	a,b
0528-250	2.141	20.70(0.08)	-1.36(0.17)	<+0.29	+0.08(0.16)	-0.49(0.18)	+0.27(0.16)	...	f,h
0551-366	1.962	20.50(0.07)	-0.96(0.11) ³	+0.85(0.07)	+0.04(0.08)	+0.03(0.06)	+0.55(0.08)	+0.23(0.10)	i
0935+417	1.373	20.52(0.10)	-1.21(0.14)	+0.21(0.14)	+0.18(0.14)	-0.37(0.14)	...	+0.33(0.18)	j,k
1104-181	1.662	20.85(0.01)	-1.59(0.02) ⁴	+0.74(0.01)	+0.20(0.01)	-0.06(0.06)	+0.60(0.02)	+0.37(0.05)	l
1122-168	0.682	20.45(0.05)	-1.40(0.05) ⁵	<+0.29	...	-0.25(0.09)	...	+0.06(0.09)	*,m
				<+0.39	...	≤-0.40(0.12)	...	≤-0.04(0.12)	*
1229-021	0.395	20.75(0.07)	<-1.32 ⁷	>+0.85	...	>+0.49	>+0.56	...	n,o
1247+267	1.223	19.87(0.09)	-1.41(0.10)	+0.39(0.16)	+0.18(0.11)	-0.17(0.07)	+0.30(0.11)	...	p
1328+307	0.692	21.25(0.06)	-1.81(0.12)	+0.61(0.14)	+0.06(0.14)	<-0.38	n,q,r
1351+318	1.149	20.23(0.10)	-1.00(0.11)	+0.76(0.11)	+0.19(0.11)	-0.04(0.07)	+0.57(0.11)	...	p
1354+258	1.420	21.54(0.06)	-2.02(0.08)	+0.43(0.11)	+0.23(0.07)	-0.29(0.07)	+0.30(0.11)	...	p
1622+238	0.656	20.36(0.10)	-1.27(0.16)	<-0.20	...	+0.41(0.16)	b,k,s
1946+769	1.738	... ¹	-1.05	<+0.23	+0.15(0.07)	-0.36(0.09)	+0.26(0.05)	...	f, t
2128-123	0.430	19.37(0.08)	>-0.78	<-0.03	...	<-0.29	*,b
2206-199	0.752	... ¹	-0.90	-0.10(0.06)	...	+0.27(0.04)	u

The numbers in parentheses are standard deviations.

¹ The total neutral hydrogen column density of these absorbers is unknown, but since $w_r(\text{Fe II } \lambda 2600)/w_r(\text{Mg II } \lambda 2796) \gtrsim 0.6$, they are at the very least moderate DLA systems. For these absorbers, a value $\log N(\text{H I}) = 20$ was adopted to estimate $[\text{Fe}/\text{H}]$.

² All the detected components of Fe II were included to estimate $[\text{Fe}/\text{H}]$, whereas it is not the case for the abundance ratios (see Sect. 4). The difference between the values of $[\text{Fe}/\text{H}]$ computed with all the components of Fe II or with only those used to derive the abundance ratios is important (> 0.12 dex) only for the DLA systems toward Q 0551-366, Q 1104-181 and Q 1122-168.

³ $z_{\text{abs}} = 1.9621$: $[\text{Fe}/\text{H}] = -1.26 \pm 0.09$.

⁴ $z_{\text{abs}} = 1.6615$: $[\text{Fe}/\text{H}] = -1.87 \pm 0.01$.

⁵ $z_{\text{abs}} = 0.6819$: $[\text{Fe}/\text{H}] = -1.83 \pm 0.06$ (components 3 + 4).

⁶ $z_{\text{abs}} = 0.6826$: $[\text{Fe}/\text{H}] = -2.23 \pm 0.05$ (component 9).

⁷ The strong Fe II lines of this multiple absorption system are saturated. A curve of growth analysis of the Fe II $\lambda\lambda 2586, 2600$ lines yields $\log N(\text{H I}) = 14.47$, thus $[\text{Fe}/\text{H}] = -1.79$.

REFERENCES: (*) This work; (a) Pettini et al. 2000; (b) Churchill et al. 2000a; (c) Vladilo et al. 1997; (d) Bergeron & D'Odorico 1986; (e) Blades et al. 1982, 1985; (f) Lu et al. 1996; (g) Petitjean & Bergeron 1994; (h) Ledoux et al. 1998; (i) Ledoux et al. 2002; (j) Meyer et al. 1995; (k) Rao & Turnshek 2000; (l) Lopez et al. 1999; (m) de la Varga et al. 2000; (n) Boissé et al. 1998; (o) Lanzetta & Bowen 1992; (p) Pettini et al. 1999; (q) Cohen et al. 1994; (r) Meyer & York 1992; (s) Steidel et al. 1997; (t) Lu et al. 1995; (u) Prochaska & Wolfe 1997b.

Table 4. Mean abundance ratios observed in DLA systems, along SMC lines of sight, and in SMC and Galactic stars:

Ratio	DLA systems ^{a,b}		SMC ^{b,c}		Galactic stars ^d	
	$0.3 < z_{\text{abs}} \leq 1.15$	$1.15 < z_{\text{abs}} < 2.2$	ISM	stars	$[\text{Fe}/\text{H}] > -0.5$	$[\text{Fe}/\text{H}] \sim -1$
[Mn/Fe]	-0.05 ± 0.28 (14)	-0.18 ± 0.22 (11)	-0.07 ± 0.05 (3)	$+0.04 \pm 0.17$	-0.06 ± 0.05	-0.26 ± 0.05
[Si/Fe]	$+0.39 \pm 0.21$ (5)	$+0.36 \pm 0.13$ (8)	$+0.82 \pm 0.25$ (3)	$+0.14 \pm 0.11$	$+0.08 \pm 0.05$	$+0.28 \pm 0.05$
[Ti/Fe]	$+0.12 \pm 0.27$ (8)	$+0.31 \pm 0.07$ (3)	$+0.28 \pm 0.37$ (2)	$+0.16 \pm 0.10$	$+0.07 \pm 0.10$	$+0.23 \pm 0.10$
[Cr/Fe]	$+0.14 \pm 0.09$ (6)	$+0.15 \pm 0.06$ (8)	$+0.12 \pm 0.04$ (3)	$+0.10 \pm 0.12$	$+0.00 \pm 0.10$	-0.02 ± 0.05
[Zn/Fe]	$+0.48 \pm 0.26$ (9)	$+0.45 \pm 0.25$ (7)	$+0.73 \pm 0.20$ (3)	$+0.08$	$+0.05 \pm 0.10$	$+0.12 \pm 0.10$

^a Results from this work. Most detection limits are significant enough (see Fig. 2) to be included in the statistics as detections.

^b The number of lines of sight involved in the computation is given in parentheses.

^c Elemental ratios observed in the ISM of the SMC (lines of sight toward Sk 155, Sk 78 and Sk 108; Welty et al. 2001) or in SMC stars (appendix of Welty et al. 1997, and refs. therein). Differences in the adopted Solar system abundances are accounted for.

^d Elemental ratios observed in Galactic halo ($[\text{Fe}/\text{H}] \sim -1$) and Galactic thin disk ($[\text{Fe}/\text{H}] > -0.5$) stars (e.g. Prochaska et al. 2000, and refs. therein).

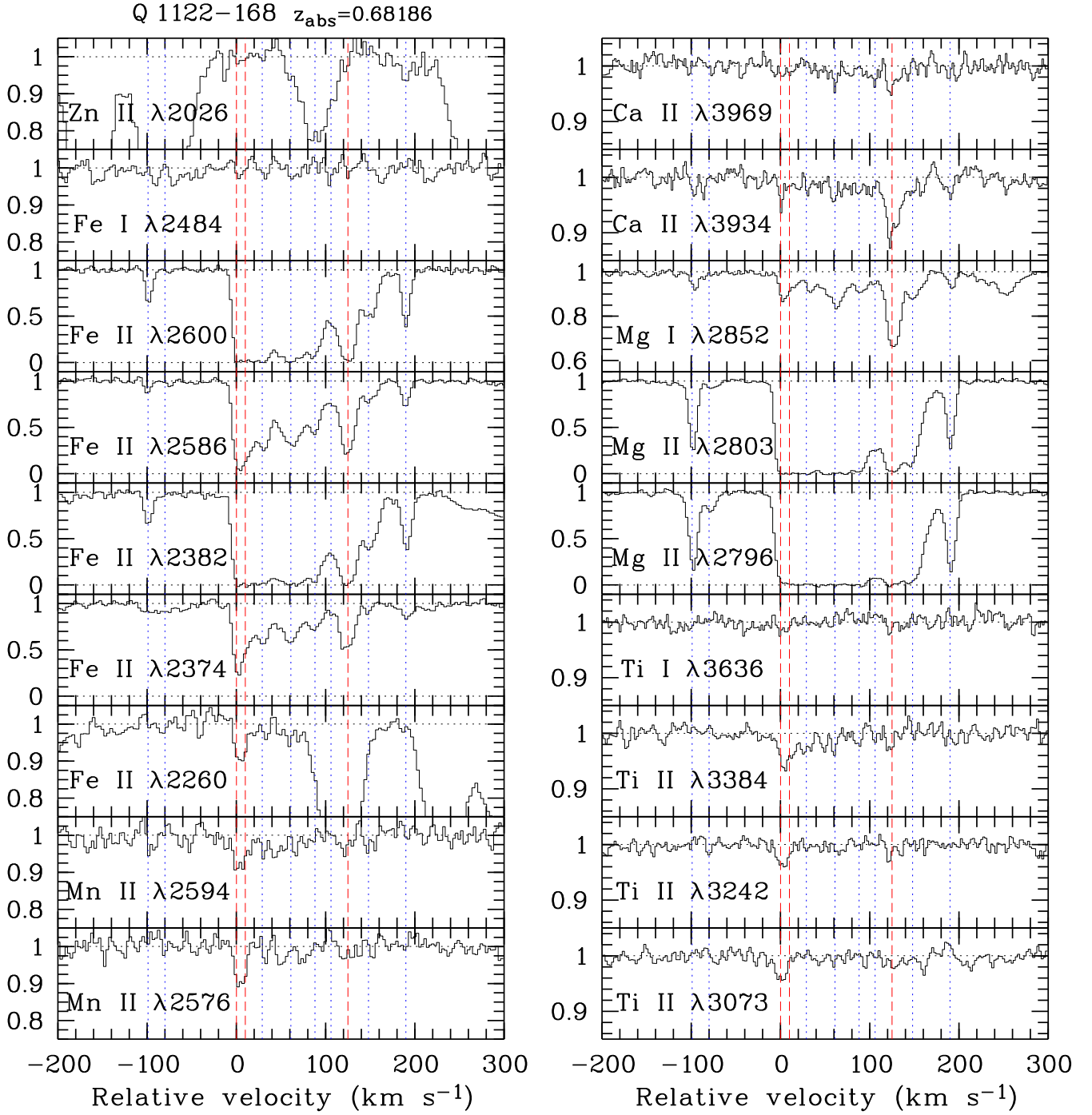


Fig. 1. Low-ionization line profiles from the $z_{\text{abs}} = 0.68186$ DLA system in the normalized VLT-UVES spectra of Q 1122–168. Individual components (see Table 2) are marked by vertical lines and the dashed lines indicate the main components used to derive elemental ratios (see text and Table 3). For this absorber, we have considered two subsystems.

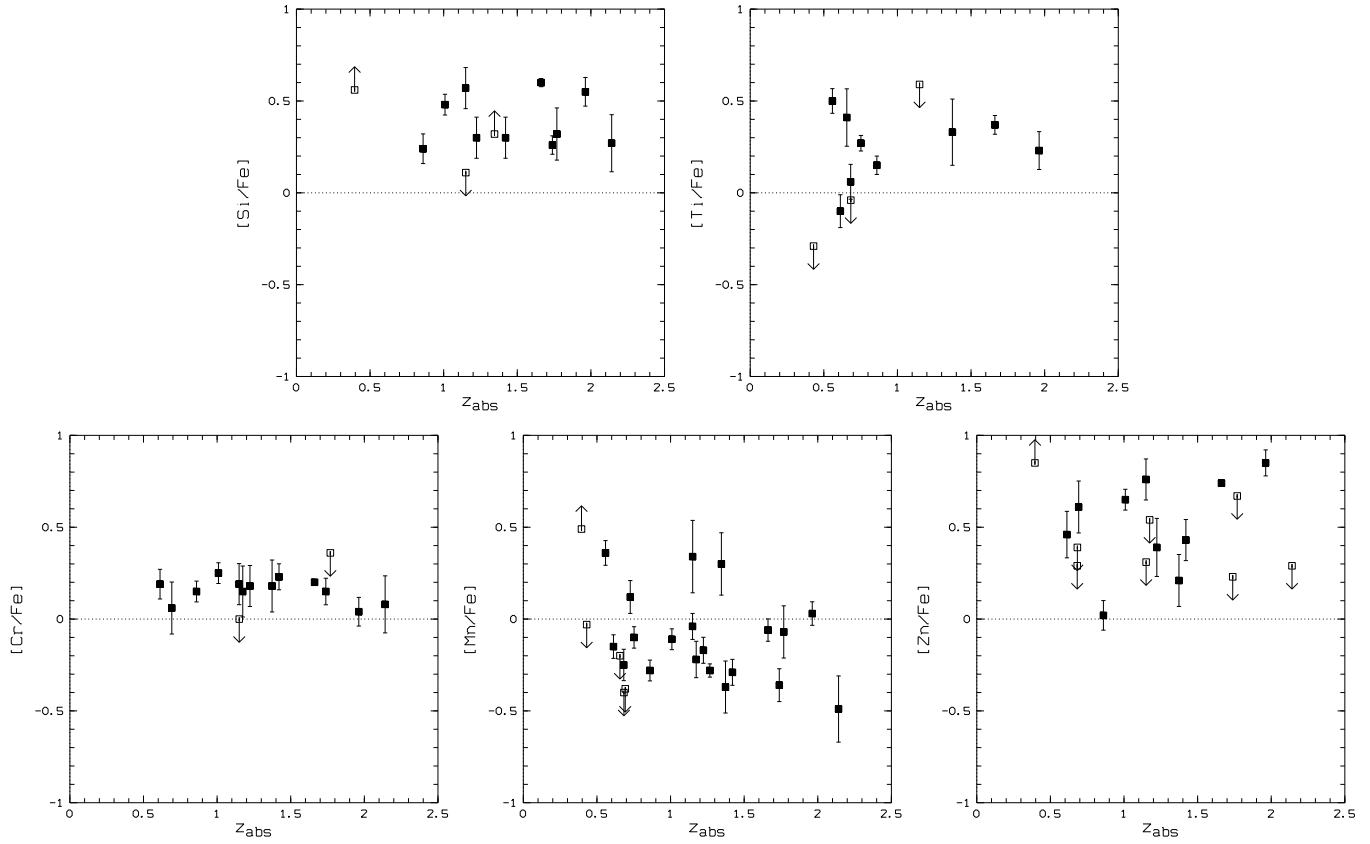


Fig. 2. Observed abundance ratios of Si, Ti, Cr, Mn and Zn relative to Fe versus redshift for DLA systems at $0.3 < z_{\text{abs}} < 2.2$. There is no apparent cosmic evolution of the abundance ratios in this redshift range.

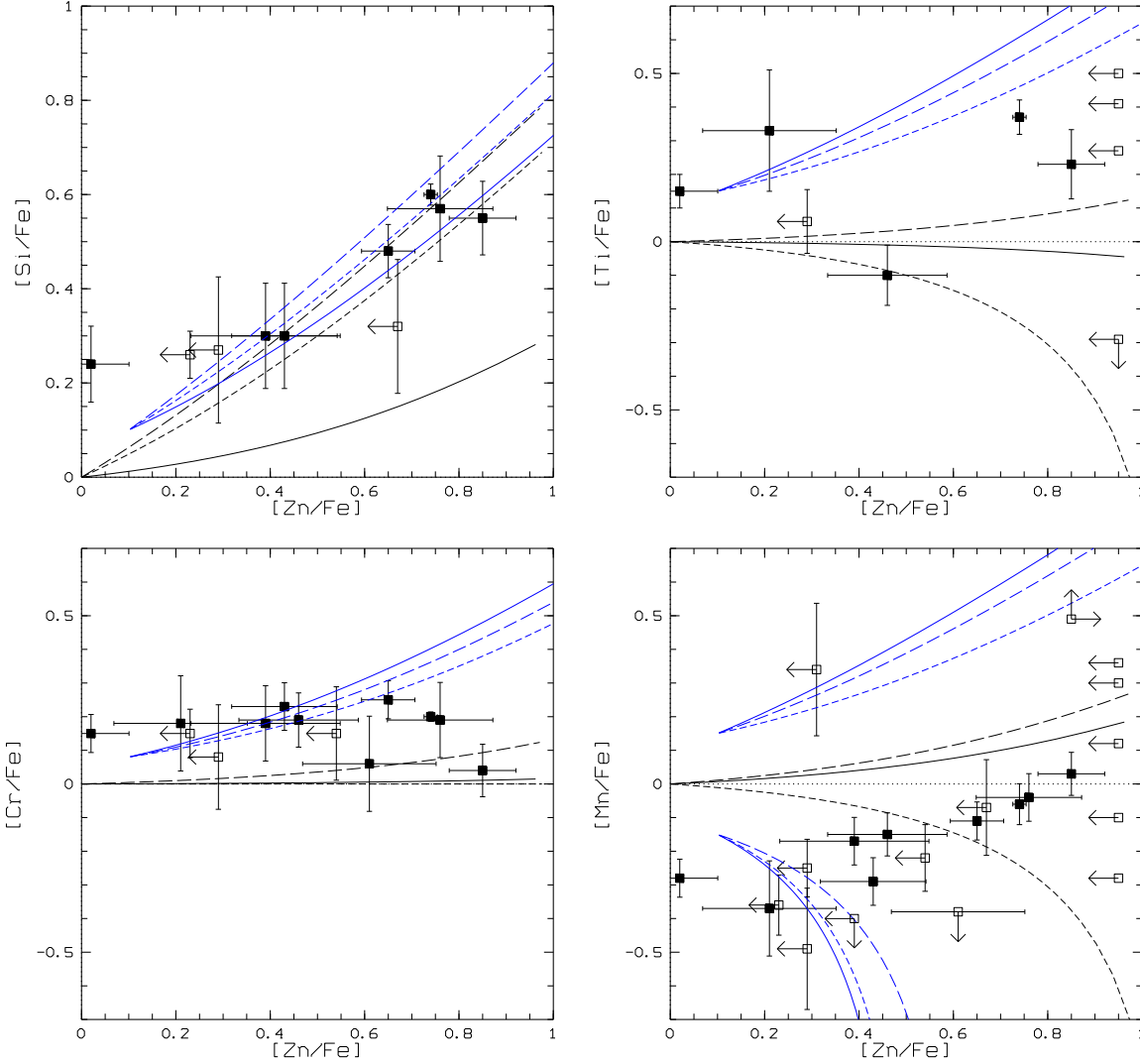


Fig. 3. Observed abundance ratios of Si, Ti, Cr and Mn relative to Fe versus observed $[Zn/Fe]$. For completeness, absorbers with Ti and/or Mn but no Zn measurements are shown assuming that $[Zn/Fe] < 0.95$. Meaningful double limits for $[Ti/Fe]$ and $[Mn/Fe]$ ratios are also displayed. Examples of depletion sequence are superimposed to the data for various dust compositions: the ISM depletion patterns of Galactic cold disk clouds (solid lines) and Galactic warm disk (long dash) and warm halo clouds (short dash) from Welty et al. (1999). Each of these sequences is given for intrinsically solar, over-solar and/or sub-solar ratios. An intrinsic $[Zn/Fe] = +0.1$ ratio is typical of those observed in Galactic halo and SMC stars (see Table 4).

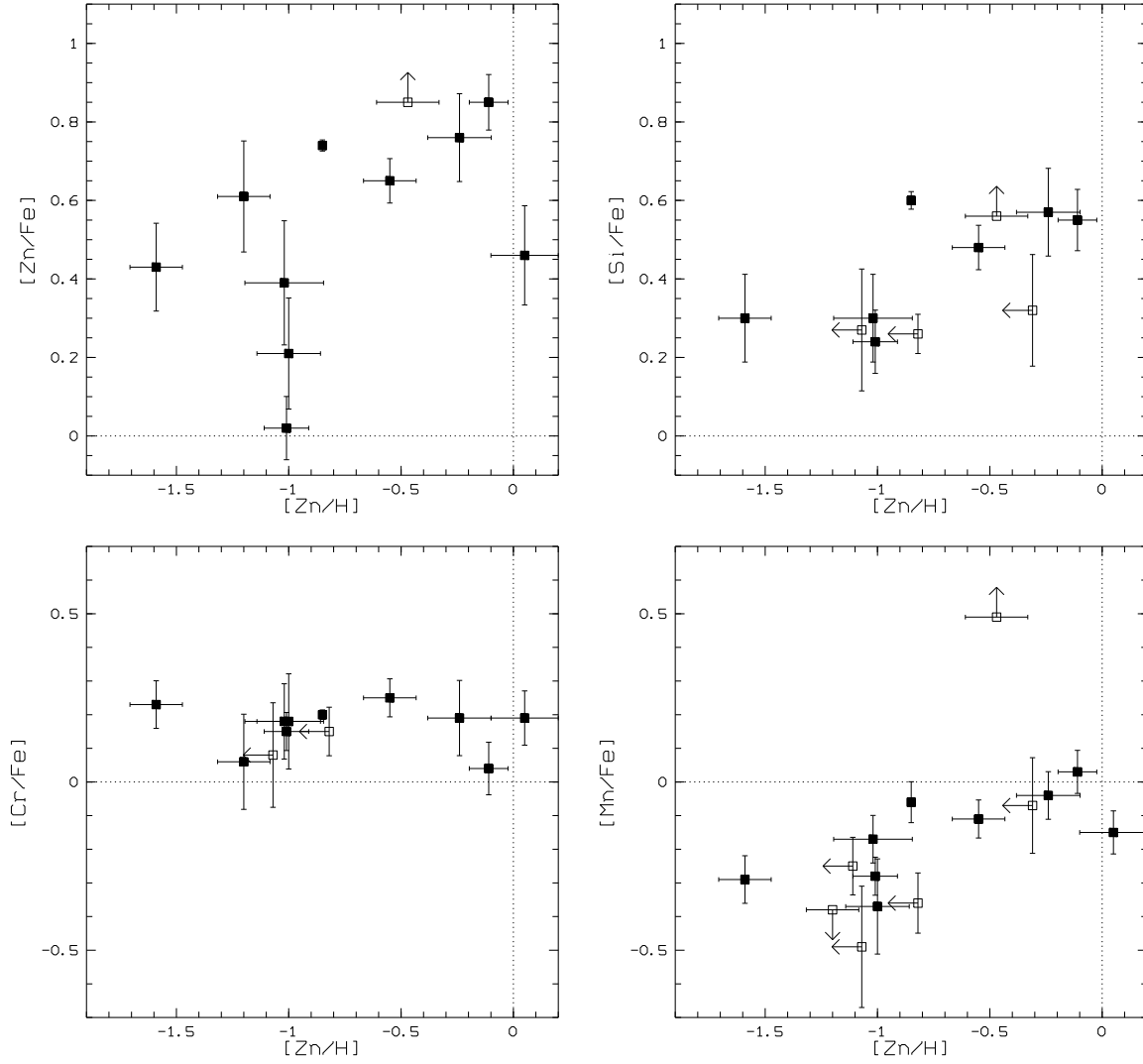


Fig. 4. Observed abundances of Zn and Si (upper panels), Cr and Mn (lower panels) relative to Fe versus the observed abundances of Zn, i.e. metallicities. Trends of increasing depletion level, traced by the observed $[Zn/Fe]$ and $[Si/Fe]$ ratios, with metallicity are present at the 1.7σ significance level for both ratios. The correlation between the observed $[Mn/Fe]$ ratio and metallicity is detected at the 2.6σ significance level.

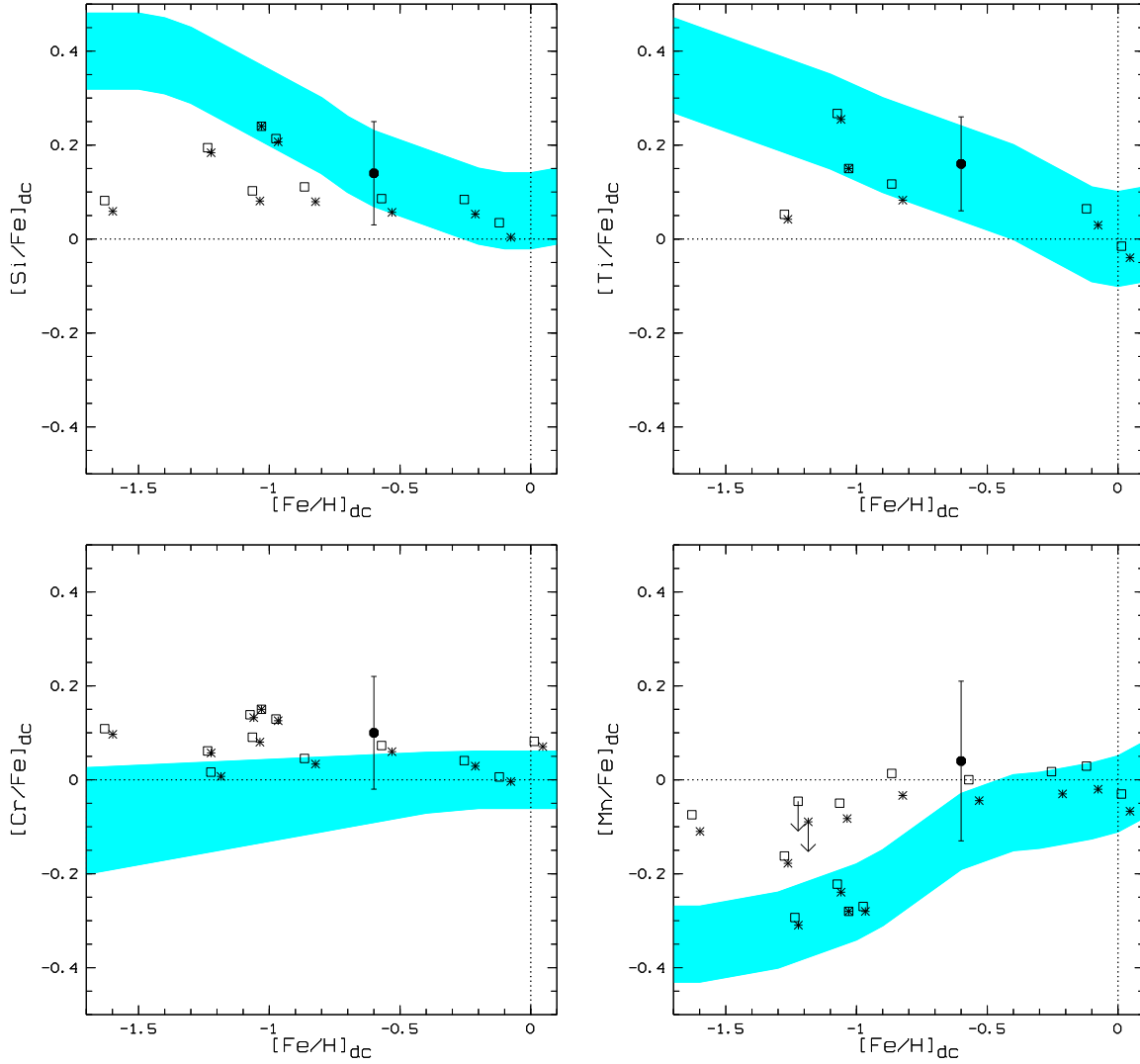


Fig. 5. Dust-corrected, i.e. intrinsic, abundance ratios of Si, Ti, Cr and Mn relative to Fe versus dust-corrected Fe abundances, i.e. metallicities. The observed $[\text{Zn}/\text{Fe}]$ ratio was used as a depletion indicator with the dust depletion patterns of Galactic warm disk (asterisks) and warm halo clouds (squares). Errors are typically ± 0.1 dex including the uncertainty in the $[\text{Zn}/\text{Fe}]$ ratios. The trends observed in Galactic stars (shaded areas) are typical values for various Galactic stellar populations and the filled circles refer to SMC stars (see Table 4).